Trilinear coupling in lead-free halide superlattice CsSnI₃/CsSiI₃: A first-principles study

Xinyu Wang [1,2] Xu Li [2,3] Yuemei Sun [1] Wenjing Yu,[1] Xiaoqin Zhu,[1] Chonggui Zhong,[4]
Hao Tian [5,*] and Liangjun Zhai [1,†]

[1]*The School of Mathematics and Physics, Jiangsu University of Technology, Changzhou 213001, China*
[2]*Laboratory of Solid State Microstructures, Nanjing University, Nanjing 210093, China*
[3]*Jiangsu Key Laboratory of Artificial Functional Materials, Department of Materials Science and Engineering,*
Nanjing University, Nanjing 210093, China
[4]*School of Sciences, Nantong University, Nantong 226007, China*
[5]*School of Physics and Electronic Engineering, Zhengzhou Normal University, Zhengzhou 450044, China*

Ferroelectricity in halide perovskites has attracted great attention, ranging from fundamental studies to technological applications. Here, we studied the structural and electrical properties of superlattice CsSnI₃/CsSiI₃ by first principles. The ground state of CsSnI₃/CsSiI₃ is a polar phase with a space group of Pc, and it possesses four trilinear couplings between polar and nonpolar modes. The Pc state is eightfold degenerate in total energy against the simultaneous inversion of couples of modes. Under an electric field, the switching of polarization is accompanied by the switching of antiferroelectric octahedral distortion tilting. Moreover, the switching barrier of CsSnI₃/CsSiI₃ can be reduced by applying a compressive strain. The unique trilinear couplings and ferroelectricity in our system suggest the potential application of lead-free halide perovskites in several energy conversion mechanisms such as piezoelectric, pyroelectric, electrical energy storage, and photovoltaic.

I. INTRODUCTION

Ferroelectric perovskite materials are well known for capacitor, sensor, memories, and energy storage applications [1–5] as well as giving rise to tremendous interest as photovoltaic and optoelectronic materials [6,7]. Ferroelectrics exhibit a spontaneous polarization that can be switched by applying an electric field. This feature usually exists in perovskite oxides where the transition-metal/oxygen bond with large polarizability is particularly favorable for promoting the transition-metal off-centering, such as BaTiO₃ and PbTiO₃ [8–10]. Compared to the perovskite oxide ferroelectrics, halide perovskites exhibit many unique properties of structural softness, light weight, and low synthesis temperatures [11]. Moreover, the halogen-based examples unlike oxides are not contraindicated by d electrons, so they allow the coexistence of ferroelectric (which requires empty d orbitals) and magnetic ordering (which requires filled d orbitals).

On the other hand, ferroelectric halide perovskites can enhance the power conversion efficiency of solar cells by improving the charge transport properties and reducing charge recombination, which shows promising optoelectronic applications [12–16]. However, the existence of ferroelectricity in halide perovskites remains controversial. For example, in tetragonal MAPbI₃, most traditional methods cannot effectively characterize its ferroelectricity and have not achieved standard saturated polarization versus electric field (*P-E*)

loops until now [17]. As a result, this work aims to increase ferroelectricity in hybrid halide perovskites and tune the semiconducting features of ferroelectrics for better device needs.

Recently, lead-free halide perovskites have attracted wide attention due to their nontoxicity and outstanding optoelectronic properties [14,18–20]. CsSnI₃, a typical lead-free inorganic perovskite, possesses a cubic or orthorhombic phase that is centrosymmetric and does not possess spontaneous polarization [21–23]. However, CsSiI₃ adopts a noncentrosymmetric structure with $R3m$ symmetry. It has been reported that superlattices of thin ferroelectric and nonferroelectric perovskite layers can possess many improved physical properties over homogeneous thin films of the same compositions [24–26]. Thus, we construct the superlattice CsSnI₃/CsSiI₃ made by centrosymmetric $Pnma$ CsSnI₃ [27] and polar $R3m$ CsSiI₃ [28]. The structures and electronic properties of the CsSnI₃/CsSiI₃ superlattice were studied by first-principles calculations and symmetry analysis. It is found that the superlattice adopts a polar ground state of Pc, and both possess the octahedral tilting of CsSnI₃ and polar distortions of CsSiI₃. Moreover, the ferroelectric polarization is not only related to the magnitude of polar distortion but closely correlated to the antipolar distortion, such as the AFD mode. Under an electric field, the polarization can be switched against the simultaneous inversion of the antipolar mode, due to the existence of trilinear couplings of lattice distortion modes in the CsSnI₃/CsSiI₃ superlattice. Furthermore, the switching barrier can be decreased by applying a compressive strain, showing unique ferroelectricity in halide perovskites.

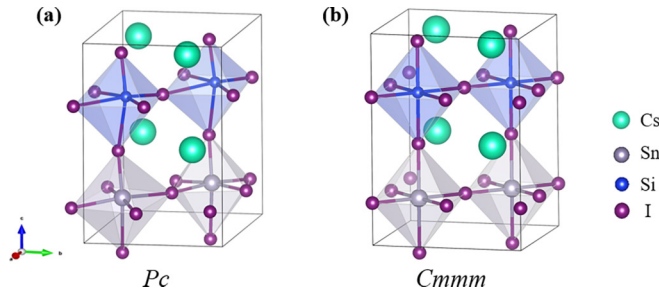*haotian@zznu.edu.cn
†zhailiangjun@jsut.edu.cn

FIG. 1. Atomic structure of ferroelectric *Pc* phase (a) and high-symmetry phase *Cmmm* (b) for CsSnI$_3$/CsSiI$_3$ superlattice.

II. COMPUTATIONAL METHODS

Density functional theory (DFT) calculations were performed by using the Vienna *ab initio* simulation package (VASP) with the projector augmented wave (PAW) method [29,30]. The following electrons were treated as valence states: Cs $5s^2\,5p^6\,6s^1$, Sn $5s^2\,5p^2$, Si $3s^2\,3p^2$, and I $5s^2\,5p^5$. A cutoff energy of 320 eV and the Perdew-Burke-Ernzerhof (PBE) exchange-correlation potential were used [31]. To simulate the CsSnI$_3$/CsSiI$_3$ superlattice, we used a $\sqrt{2} \times \sqrt{2} \times 2$ supercell containing 20 atoms. The atomic positions were relaxed using the Monkhorst-Pack k meshes of 0.2 Å^{-1}. Electronic relaxations converged within 10^{-8} eV and ionic relaxation was performed until the residual force was 1 meV Å^{-1}. Spontaneous polarizations were calculated by using the Berry phase method [32]. Considering the effect of an electric field, the electric enthalpy functional $F(\mathbf{R}, \mathcal{E}) = E_{\mathrm{KS}}^0(\mathbf{R}) - P(\mathbf{R}) \cdot \mathcal{E}$ in Ref. [33] was used to describe the response of structural and electric properties to an electric field. Here, $\mathcal{E}$ is the applied electric field, $E_{\mathrm{KS}}^0(\mathbf{R})$ is the zero-field ground-state Kohn-Sham energy at coordinates $\mathbf{R}$, and P is the corresponding electronic polarization. In the presence of an applied electric field, the equilibrium coordinates that minimize the electric enthalpy functional should satisfy the force-balance equation $-\frac{dE_{\mathrm{KS}}^0}{dR} + \mathbf{Z}^0 \cdot \mathcal{E} = 0$, where $\mathbf{Z}^0$ is the zero-field Born effective charge tensor. This scheme has been successfully verified for the study of electric field related physical responses in ferroelectric and multiferroic compounds [26,33]. For epitaxial strain, the in-plane lattice constants were fixed and the atomic positions and out of plane lattice constants of the superlattice have been relaxed.

III. RESULTS AND DISCUSSION

CsSnI$_3$ possesses an orthorhombic nonpolar phase *Pnma* with iodine antiferrodistortive (AFD) octahedra motions, having in-plane antiphase tilts and out of plane in-phase tilt ($a^-a^-c^+$ tilts in Glazer notation [34]). The ground state of CsSiI$_3$ is a rhombohedral polar *R3m* structure. Figure 1(a) shows the structure of the [CsSnI$_3$]$_1$/[CsSiI$_3$]$_1$ superlattice, which possesses the ground state of the *Pc* phase. The structures of CsSiI$_3$ and CsSnI$_3$/CsSiI$_3$ are dynamically stable with no imaginary phonon frequency in Fig. S2 in the Supplemental Material [35] (also see [36,37]). Meanwhile, the superlattice CsSnI$_3$/CsSiI$_3$ is a periodic structure,

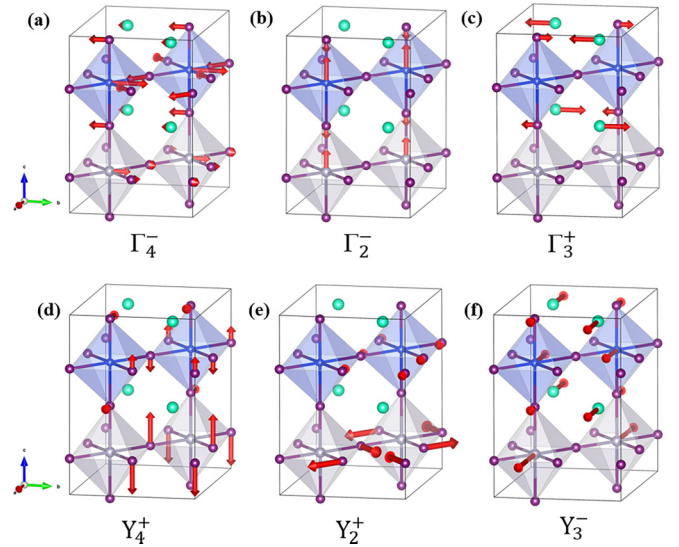FIG. 2. Sketch of distortion mode Γ_4^- (a), Γ_2^- (b), Γ_3^+ (c), Y_4^+ (d), Y_2^+ (e) and Y_3^- (f) in CsSnI$_3$/CsSiI$_3$ superlattice.

alternating the corresponding component along one direction infinitely in the calculations. This perfect order superlattice can be grown by molecular beam epitaxy (MBE) and pulsed-laser assisted (PLA) technology [38–42]. Symmetry mode analysis using AMPLIMODES [43] has been performed on the CsSnI$_3$/CsSiI$_3$ superlattice; the ground state *Pc* consists of a combination of several lattice distortions of high-symmetry superlattice. The high-symmetry phase can be found by using the pseudosymmetry searching software PSEUDO [44]. In Fig. 1(b), the *Cmmm* phase is considered as the high-symmetry structure. Six main lattice distortions decomposed from the *Pc* ground state can be distinguished with symmetries labeled as Γ_4^-, Γ_2^-, Γ_3^+, Y_4^+, Y_2^+, and Y_3^-. Figures 2(a)–2(f) display the pattern of atomic displacements related to these distortion modes. Figure 2(a) shows the in-plane polar mode Γ_4^- where Sn and Si cations move along the *b* direction, and I anions mainly move along the $-b$ direction, resulting in polarization along the *b* direction. Figure 2(b) shows the out of plane polar mode Γ_2^- along the *c* direction. Figure 2(c) shows the antipolar distortions Γ_3^+ with the *A*-site cation displacements along the *a* direction, corresponding to the distortion mode X$_5^+$ of the $Pm\bar{3}m$ phase decomposed from nonpolar structure *Pnma* for CsSnI$_3$. Figures 1(d) and 1(e) show the out of phase in-plane octahedral tilting mode Y_4^+ and the in phase of the out of plane octahedral tilting mode Y_2^+. The two tilting modes are similar to the AFD R$_4^+$ and M$_2^+$ in CsSnI$_3$. We find that the Y_2^+ distortion mode is mainly contributed by Sn-centered I$_6$ octahedra while the Si-centered I$_6$ octahedra tilting almost can be ignored. Moreover, there is another antipolar distortion mode Y_3^- [Fig. 1(f)]. In the Y_3^- mode, atoms in the CsI layer and Sn/Si atoms possess displacements along the *a* direction.

We then analyze the effect of each mode on the ferroelectric behavior in the superlattice CsSnI$_3$/CsSiI$_3$. From the absolute amplitude of each mode, we find the strongest contribution comes from the two tilting modes Y_4^+ and Y_2^+ with
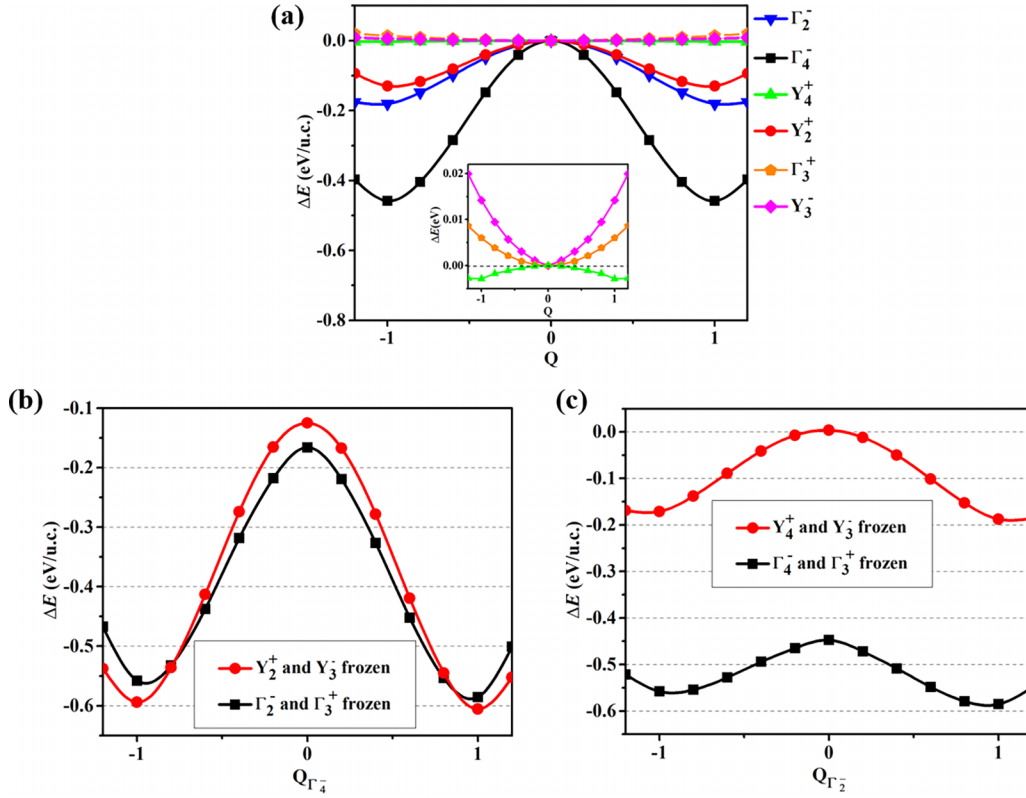
FIG. 3. (a) The total energy with respect to the amplitude of the Γ_4^-, Γ_2^-, Γ_3^+, Y_4^+, Y_2^+, and Y_3^- modes. (b) Energy as a function of the amplitude of the Γ_4^- mode when freezing Y_2^+ and Y_3^- (red line), and Γ_2^- and Γ_3^+ (black line). (c) Energy as a function of the amplitude of the Γ_2^- mode when freezing Y_4^+ and Y_3^- (red line), and Γ_4^- and Γ_3^+ (black line). The amplitudes Q are normalized corresponding to the relaxed structure. Here, we set the energy of the *Cmmm* phase to zero. The location of the minima in (b), (c) can refer to the dotted lines.

large amplitudes of 1.46 and 0.6 Å. The next largest contributions are from the polar modes Γ_4^- and Γ_2^- with amplitudes of 0.5 and 0.4 Å. Thus, the Y_4^+ and Y_2^+ modes are the primary structural distortions, which lower the symmetry of the prototype phase to *Pmna* and *Pbam*. Note that both of them are nonpolar subgroups and insufficient to break the inversion symmetry. The secondary induced polar distortions in the Γ_4^- and Γ_2^- modes are allowed to reduce the symmetry to *Pc*. This means that the coupling of two tilting modes can induce polar

distortions, though they cannot yield polarization by themselves. On the other hand, there are also small contributions from the antipolar modes Γ_3^+ and Y_3^-. To further study the driving forces for, and competition between polar and nonpolar structural distortions, the ISOTROPY software package [45] is used to derive the expression of energetic terms that are possible by symmetry in the presently reported *Pc* state of the CsSnI$_3$/CsSiI$_3$ superlattice. We identify the following couplings:

$$
\begin{aligned}
E = E_0 &+ A_1 Q_{\Gamma_2^-} Q_{\Gamma_4^-} Q_{\Gamma_3^+} + A_2 Q_{\Gamma_2^-} Q_{Y_4^+} Q_{Y_3^-} + A_3 Q_{\Gamma_4^-} Q_{Y_2^+} Q_{Y_3^-} + A_4 Q_{\Gamma_3^+} Q_{Y_2^+} Q_{Y_4^+} + B_1 Q_{\Gamma_2^-}^2 + B_2 Q_{\Gamma_4^-}^2 + B_3 Q_{\Gamma_3^+}^2 \\
&+ B_4 Q_{Y_4^+}^2 + B_5 Q_{Y_2^+}^2 + B_6 Q_{Y_3^-}^2 + C_1 Q_{\Gamma_2^-}^4 + C_2 Q_{\Gamma_2^-}^2 Q_{\Gamma_4^-}^2 + C_3 Q_{\Gamma_4^-}^4 + C_4 Q_{\Gamma_2^-}^2 Q_{\Gamma_3^+}^2 + C_5 Q_{\Gamma_4^-}^2 Q_{\Gamma_3^+}^2 \\
&+ C_6 Q_{\Gamma_3^+}^4 + C_7 Q_{\Gamma_2^-}^2 Q_{Y_2^+}^2 + C_8 Q_{\Gamma_4^-}^2 Q_{Y_2^+}^2 + C_9 Q_{\Gamma_3^+}^2 Q_{Y_2^+}^2 + C_{10} Q_{Y_2^+}^4 + \ldots ,
\end{aligned}
\tag{1}
$$

where the $Q_{\Gamma_4^-}$, $Q_{\Gamma_2^-}$, $Q_{\Gamma_3^+}$, $Q_{Y_4^+}$, $Q_{Y_2^+}$, and $Q_{Y_3^-}$ represent the amplitude of the Γ_4^-, Γ_2^-, Γ_3^+, Y_4^+, Y_2^+, and Y_3^- modes, respectively. The ($Q_{\Gamma_2^-}$, $Q_{\Gamma_4^-}$, $Q_{Y_2^+}$, $Q_{Y_4^+}$, $Q_{\Gamma_3^+}$, $Q_{Y_3^-}$) of the *Pc* state is (1, 1, 1, 1, 1, 1). The antipolar distortion Γ_3^+ is allowed by the condensation of two rotational modes Y_4^+ and Y_2^+, which is similar to the trilinear coupling of $Q_{X_5^+} Q_{R_4^+} Q_{M_2^+}$ in *Pnma* structure [46]. The two types of trilinear couplings, $Q_{\Gamma_2^-} Q_{Y_4^+} Q_{Y_3^-}$ and $Q_{\Gamma_4^-} Q_{Y_2^+} Q_{Y_3^-}$, suggest that the AFD and antipolar motions may modify the polariza-

tion. Moreover, the term $Q_{\Gamma_2^-} Q_{\Gamma_4^-} Q_{\Gamma_3^+}$ represents a coupling between in-plane polar mode Γ_4^- and out of plane polar mode Γ_2^-.

To confirm this scenario, we calculate the total energy as a function of the normalized amplitude Q of each mode shown in Fig. 3(a). For the Γ_4^-, Γ_2^-, Y_4^+, and Y_2^+ modes, their energy curves have a characteristic double-well shape, indicating that they can be unstable at the symmetry phase *Cmmm*. However, the energy variation of modes Γ_3^+ and Y_3^- are stable as a single
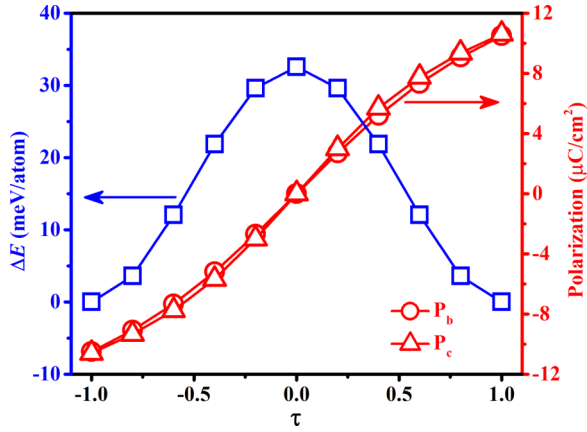
FIG. 4. Total energy difference between ferroelectric and paraelectric phase as a function of the parameter τ (left axis) and the evolution of polarization from positive to negative ferroelectric states calculated by the Berry phase method (right axis).

well in the curve of energy as a function of its amplitude [inset of Fig. 3(a)]. Interestingly, when freezing Y_2^+ and Y_3^- with their amplitude in the Pc ground state, the energy gain of Γ_4^- distortion is much more than that without other modes frozen [see Figs. 3(a) and 3(b)]. The simultaneous condensation of the Y_4^+ and Y_3^- modes can also increase the energy gain of polar mode Γ_2^- in Fig. 3(c). Moreover, the asymmetrical energy curves in Figs. 3(b) and 3(c) show that the P and $-P$ states are not energetically equivalent, indicating the existence of trilinear couplings in the superlattice. The coefficients of four trilinear coupling terms can be obtained by fitting these energy curves with Eq. (1): $A_1 = -0.019$, $A_2 = -0.011$, $A_3 = -0.005$, and $A_4 = -0.018$ eV/unit cell (u.c.). The larger value of A_1 shows that two polar modes Γ_4^- and Γ_2^- have a strong coupling with each other as shown in Figs. 3(b) and 3(c). When freezing one polar mode and antipolar mode Γ_3^+, the energy gain of another polar mode can be markedly increased. On the other hand, these trilinear couplings in Eq. (1) prevent the degeneracy of the Pc against the simultaneous inversion of each mode; thus the phases of $(1, 1, 1, 1, 1, 1)$ and $(-1, -1, -1, -1, -1, -1)$ are not energetically equivalent, which is consistent with the calculated results in Fig. S5(b) [35]. However, the Pc is eightfold degenerate in total energy

TABLE I. The phases $(Q_{\Gamma_2^-}, Q_{\Gamma_4^-}, Q_{Y_2^+}, Q_{Y_4^+}, Q_{\Gamma_3^+}, Q_{Y_3^-})$ with the same total energy in the Pc state.

	Polar modes		AFD modes		Antipolar modes	
	$Q_{\Gamma_2^-}$	$Q_{\Gamma_4^-}$	$Q_{Y_2^+}$	$Q_{Y_4^+}$	$Q_{\Gamma_3^+}$	$Q_{Y_3^-}$
Phase 1	1	1	1	1	1	1
Phase 2	1	−1	−1	1	−1	1
Phase 3	−1	−1	1	1	1	−1
Phase 4	−1	1	1	−1	−1	1
Phase 5	1	1	−1	−1	1	−1
Phase 6	−1	−1	−1	−1	1	1
Phase 7	−1	1	−1	1	−1	−1
Phase 8	1	−1	1	−1	−1	−1

against the simultaneous inversion of couples of modes, and the phases from 1 to 8 have the same total energy according to our calculations in Table I. The results show that a reversal of the polarization should be accompanied by the reversal of the AFD and antipolar modes to end up in a Pc minimum having the same energy, implying a hybrid improper ferroelectric in the $CsSnI_3/CsSiI_3$ superlattice.

As a next step in the analysis, we estimate the value of ferroelectric polarization in the $CsSnI_3/CsSiI_3$ superlattice. Here, a phase $P2_1/c$ composed of AFD (Y_2^+ and Y_4^+) and antipolar distortion Γ_3^+ can be considered as the paraelectric state ($\tau = 0$), according to the energy degenerate states phase 1 and phase 3. Comparing to a virtual paraelectric state $P2_1/c$ ($\tau = 0$) composed of AFD (Y_2^+ and Y_4^+) and antipolar distortion Γ_3^+, the ferroelectric state ($\tau = 1$) includes the sum of distortion components $\Gamma_4^- + \Gamma_2^- + Y_3^-$ leading to the polar phase Pc. This parameter τ expresses a scaling parameter of atomic displacements. The state of $\tau = -1$ ($-P$) possesses the opposite atomic displacements of those in the $\tau = 1$ state (P), resulting from a switching of the distortion modes Γ_4^-, Γ_2^-, and Y_3^-. Figure 4 shows the energy variation from the ferroelectric state to the paraelectric state as a function of τ. We set the energy of state $\tau = 0$ to be zero. The energy curve exhibits a convex and symmetrical shape between the P and $-P$ states, which is consistent with the energetically equivalent states of phase 1 and phase 3 in Table I. Moreover, the results show that the $CsSnI_3/CsSiI_3$ superlattice possesses an energy
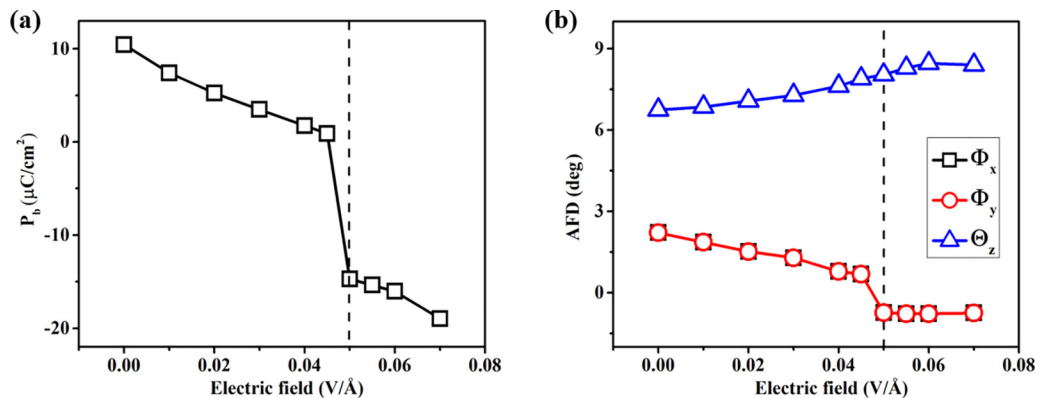

FIG. 5. (a) The ferroelectric polarization and (b) AFD octahedral tilting angles with applying an electric field from 0 to 0.08 eV/Å along the $-b$ direction.
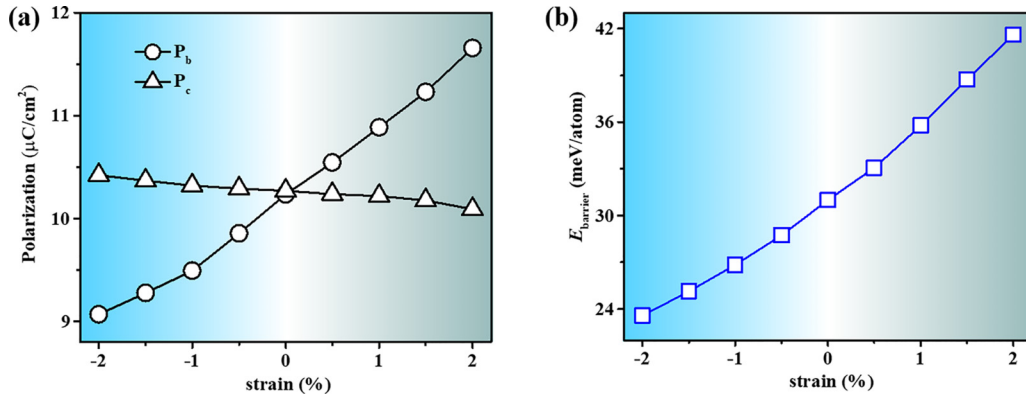
FIG. 6. (a) The ferroelectric polarization and (b) the switching barrier during the process of ferroelectric switching as a function of strain.

barrier (33 meV/atom) of switching ferroelectric polarization switching barrier from the P to the $-P$ states. Furthermore, we calculate the variation of polarizations from positive to negative ferroelectric states by the Berry phase method detailed in Fig. S6 [35]. The in-plane polarization and out of plane polarization are approximately 10.2 and 10.3 μC/cm^2, which are calculated from the polarization difference of the ferroelectric state ($\tau = 1$) and paraelectric state ($\tau = 0$).

Since the ferroelectric polarization is strongly sensitive to the electric field, we consider the situation of applying an electric field to the CsSnI$_3$/CsSiI$_3$ superlattice. Under an electric field along $-b$ ranging from 0 to 0.07 V/Å, we calculate the variation of polarization and AFD angles (Φ_x, Φ_y, Θ_z) as shown in Figs. 5(a) and 5(b). Here, we average the AFD angles of SnI$_6$ and SiI$_6$ octahedra. It can be seen that the value of polarization decreases with increasing the electric field, as well as the direction of polarization is switched to $-b$ when the electric field reaches 0.05 V/Å. Here, the opposite signs of polarization represent the switching of polarization from b to $-b$. When releasing the large electric field, the negative polarization can be modified (without a change of direction) and has the same magnitude as the initial zero-field state. Figure 5(b) shows that the out of plane AFD in-phase angle Θ_z increases with the increase of the electric field. However, the variation of in-plane AFD antiphase angles presents a similar trend to the polarization curve. We also discover that the Φ_x and Φ_y are reversed with the switching of polarization at an electric field of 0.05 V/Å. The simultaneous inversion of the polar mode and the AFD octahedra distortion mode under an electric field originates from trilinear couplings of $Q_{\Gamma_4^-} Q_{Y_2^+} Q_{Y_3^-}$ and $Q_{\Gamma_3^+} Q_{Y_2^+} Q_{Y_4^+}$ in Eq. (1), corresponding to phase 8 in Table I. This result is different from the other ferroelectric superlattices, such as BiFeO$_3$/NdFeO$_3$, BiFeO$_3$/LaFeO$_3$, and PbTiO$_3$/LaTiO$_3$ [26,47,48], in which the switching of in-plane polarization is accompanied by the reversal of out of plane AFD octahedral tilting, corresponding to phase 2 in Table I.

We further investigate the strain effect on the electric properties of the CsSnI$_3$/CsSiI$_3$ superlattice. Figures 6(a) and 6(b) show the ferroelectric polarization and switching barrier E_{barrier} of CsSnI$_3$/CsSiI$_3$ during the process of ferroelectric switching with different strains. It can be seen that the in-plane polarization decreases with the increase of compressive strain and increases with the increase of tensile strain. However,

the out of plane polarization exhibits an opposite variation with in-plane polarization as a function of strain. As the modulation of ferroelectric and structural properties occurs by applying strain, the switching barrier decreases with the increase of compressive strain and increases with the increase of tensile strain. The switching barrier reduced by 33% under a compressive strain of -2% presents the ideal ferroelectric properties, indicating a promising application.

IV. CONCLUSIONS

The structural and electric properties of the CsSnI$_3$/CsSiI$_3$ superlattice have been investigated by first-principles methods. The CsSnI$_3$/CsSiI$_3$ superlattice possesses a noncentrosymmetric structure with a space group of Pc. The ferroelectric feature of this superlattice has been observed with the in-plane polarization of 10.2 μC/cm^2 and the out of plane polarization of 10.3 μC/cm^2 by Berry phase calculation. Moreover, we found that four types of trilinear couplings between polar (Γ_4^-, Γ_2^-), AFD (Y_4^+, Y_2^+), and antiferroelectric (Γ_3^+, Y_3^-) distortion modes have a significant influence on ferroelectric polarization. As an electric field was applied to the CsSnI$_3$/CsSiI$_3$ superlattice, the polarization was switched inducing the opposite of AFD (in-phase) angles. We further obtained the reduced ferroelectric switching barrier with the effect of compressive strain. Our findings exhibit a unique ferroelectric halide superlattice and broaden its potential application for energy conversion devices.

[1] J. Seidel, D. Fu, S.-Y. Yang, E. Alarcón-Lladó, J. Wu, R. Ramesh, and J. W. Ager III, Phys. Rev. Lett. **107**, 126805 (2011).

[2] I. M. McKinley, F. Y. Lee, and L. Pilon, Appl. Energy **126**, 78 (2014).

[3] C. R. Bowen, J. Taylor, E. LeBoulbar, D. Zabek, A. Chauhan, and R. Vaish, Energy Environ. Sci. **7**, 3836 (2014).

[4] A. Chauhan, S. Patel, G. Vats, and R. Vaish, Energy Technol. **2**, 205 (2014).

[5] R. Sao, G. Vats, and R. Vaish, Ferroelectrics **474**, 1 (2015).

[6] I. Grinberg, D. V. West, M. Torres, G. Gou, D. M. Stein, L. Wu, G. Chen, E. M. Gallo, A. R. Akbashev, and P. K. Davies, Nature (London) **503**, 509 (2013).

[7] Y. Bai, P. Tofel, J. Palosaari, H. Jantunen, and J. Juuti, Adv. Mater. **29**, 1700767 (2017).

[8] V. Bhide, K. Deshmukh, and M. Hegde, Physica (Amsterdam) **28**, 871 (1962).

[9] R. E. Cohen and H. Krakauer, Ferroelectrics **136**, 65 (1992).

[10] M. Okuyama and Y. Hamakawa, Ferroelectrics **63**, 243 (1985).

[11] S. Horiuchi and Y. Tokura, Nat. Mater. **7**, 357 (2008).

[12] Y. Liu, D. Kim, A. V. Ievlev, S. V. Kalinin, M. Ahmadi, and O. S. Ovchinnikova, Adv. Funct. Mater. **31**, 2102793 (2021).

[13] W. Zheng, X. Wang, X. Zhang, B. Chen, H. Suo, Z. Xing, Y. Wang, H. L. Wei, J. Chen, and Y. Guo, Adv. Mater. **35**, 2205410 (2022).

[14] W. Ning and F. Gao, Adv. Mater. **31**, 1900326 (2019).

[15] S. Shahrokhi, W. Gao, Y. Wang, P. R. Anandan, M. Z. Rahaman, S. Singh, D. Wang, C. Cazorla, G. Yuan, and J. M. Liu, Small Methods **4**, 2000149 (2020).

[16] W.-Q. Liao, Y. Zhang, C.-L. Hu, J.-G. Mao, H.-Y. Ye, P.-F. Li, S. D. Huang, and R.-G. Xiong, Nat. Commun. **6**, 7338 (2015).

[17] M. N. F. Hoque, M. Yang, Z. Li, N. Islam, X. Pan, K. Zhu, and Z. Fan, ACS Energy Lett. **1**, 142 (2016).

[18] J. Li, J. Duan, X. Yang, Y. Duan, P. Yang, and Q. Tang, Nano Energy **80**, 105526 (2021).

[19] X. Li, X. Gao, X. Zhang, X. Shen, M. Lu, J. Wu, Z. Shi, V. L. Colvin, J. Hu, and X. Bai, Adv. Sci. **8**, 2003334 (2021).

[20] F. Cao and L. Li, Adv. Funct. Mater. **31**, 2008275 (2021).

[21] K. Shum, Z. Chen, J. Qureshi, C. Yu, J. J. Wang, W. Pfenninger, N. Vockic, J. Midgley, and J. T. Kenney, Appl. Phys. Lett. **96**, 221903 (2010).

[22] I. Chung, J.-H. Song, J. Im, J. Androulakis, C. D. Malliakas, H. Li, A. J. Freeman, J. T. Kenney, and M. G. Kanatzidis, J. Am. Chem. Soc. **134**, 8579 (2012).

[23] L. Y. Huang and W. R. L. Lambrecht, Phys. Rev. B **88**, 165203 (2013).

[24] N. Sai, B. Meyer, and D. Vanderbilt, Phys. Rev. Lett. **84**, 5636 (2000).

[25] M. P. Warusawithana, E. V. Colla, J. N. Eckstein, and M. B. Weissman, Phys. Rev. Lett. **90**, 036802 (2003).

[26] L. Chen, C. Xu, H. Tian, H. Xiang, J. Íñiguez, Y. Yang, and L. Bellaiche, Phys. Rev. Lett. **122**, 247701 (2019).

[27] R. J. Sutton, M. R. Filip, A. A. Haghighirad, N. Sakai, B. Wenger, F. Giustino, and H. J. Snaith, ACS Energy Lett. **3**, 1787 (2018).

[28] S. K. Radha and W. R. Lambrecht, Phys. Status. Solidi. **216**, 1800962 (2019).

[29] P. E. Blochl, Phys. Rev. B **50**, 17953 (1994).

[30] G. Kresse and J. Furthmuller, Comput. Mater. Sci. **6**, 15 (1996).

[31] J. P. Perdew, K. Burke, and M. Ernzerhof, Phys. Rev. Lett. **77**, 3865 (1996).

[32] R. D. King-Smith and D. Vanderbilt, Phys. Rev. B **47**, 1651 (1993).

[33] H. Fu and L. Bellaiche, Phys. Rev. Lett. **91**, 057601 (2003).

[34] A. M. Glazer, Acta Crystallogr., Sect. B **28**, 3384 (1972).

[35] See Supplemental Material at http://link.aps.org/supplemental/10.1103/PhysRevB.108.195204 which includes Refs. [36,37] and the structural and ferroelecric properties; the band structure can be found in the Supplemental Material.

[36] H. T. Stokes and D. M. Hatch, J. Appl. Crystallogr. **38**, 237 (2005).

[37] J. B. Neaton, C. Ederer, U. V. Waghmare, N. A. Spaldin, and K. M. Rabe, Phys. Rev. B **71**, 014113 (2005).

[38] T. Harman, P. Taylor, M. Walsh, and B. LaForge, Science **297**, 2229 (2002).

[39] L. Goldstein, F. Glas, J. Marzin, M. Charasse, and G. Le Roux, Appl. Phys. Lett. **47**, 1099 (1985).

[40] R. Singh, R. Kottokkaran, V. L. Dalal, and G. Balasubramanian, Nanoscale **9**, 8600 (2017).

[41] H. N. Lee, H. M. Christen, M. F. Chisholm, C. M. Rouleau, and D. H. Lowndes, Nature (London) **433**, 395 (2005).

[42] M. S. Gudiksen, L. J. Lauhon, J. Wang, D. C. Smith, and C. M. Lieber, Nature (London) **415**, 617 (2002).

[43] D. Orobengoa, C. Capillas, M. I. Aroyo, and J. M. Perez-Mato, J. Appl. Crystallogr. **42**, 820 (2009).

[44] E. Kroumova, M. Aroyo, J. Perez-Mato, S. Ivantchev, J. Igartua, and H. Wondratschek, J. Appl. Crystallogr. **34**, 783 (2001).

[45] D. M. Hatch and H. T. Stokes, J. Appl. Crystallogr. **36**, 951 (2003).

[46] S. Amisi, E. Bousquet, K. Katcho, and P. Ghosez, Phys. Rev. B **85**, 064112 (2012).

[47] Z. Zanolli, J. C. Wojdeł, J. Íñiguez, and P. Ghosez, Phys. Rev. B **88**, 060102(R) (2013).

[48] B. Xu, D. Wang, H. J. Zhao, J. Íñiguez, X. M. Chen, and L. Bellaiche, Adv. Funct. Mater. **25**, 3626 (2015).